molecules

MDPI

Article

Study on Extraction Valuable Metal Elements by Co-Roasting Coal Gangue with Coal Gasification Coarse Slag

Jincheng Zhao [1,2,3], Tao Yu [1,2,3,*], Huan Zhang [1], Yu Zhang [1], Lanting Ma [1,3], Jinling Li [2,3], Chengtun Qu [1,2] and Te Wang [2,3]

[1] Yan'an Key Laboratory of Low Carbon Synergistic Control Technology and Reservoir Protection for Oil and Gas Field Environmental Pollution, Shaanxi Fuquan Environmental Protection Technology Co., Ltd., Yan'an 727500, China; 21211070886@stumail.xsyu.edu.cn (J.Z.); zhuan@wnu.edu.cn (H.Z.); zhangyu@xynu.edu.cn (Y.Z.); malanting2020@xsyu.edu.cn (L.M.); xianquct@xsyu.edu.cn (C.Q.)

[2] State Key Laboratory of Petroleum Pollution Control, College of Chemistry and Chemical Engineering, Xi'an Shiyou University, Xi'an 710065, China; lijinling@xsyu.edu.cn (J.L.); 21212070982@stumail.xsyu.edu.cn (T.W.)

[3] Shaanxi Oil and Gas Pollution Control and Reservoir Protection Key Laboratory, College of Chemistry and Chemical Engineering, Xi'an Shiyou University, Xi'an 710065, China

* Correspondence: 180708@xsyu.edu.cn

Abstract: Coal gangue (CG) and coal gasification coarse slag (CGCS) possess both hazardous and resourceful attributes. The present study employed co-roasting followed by H_2SO_4 leaching to extract Al and Fe from CG and CGCS. The activation behavior and phase transformation mechanism during the co-roasting process were investigated through TG, XRD, FTIR, and XPS characterization analysis as well as Gibbs free energy calculation. The results demonstrate that the leaching rate of total iron (TFe) reached 79.93%, and Al^{3+} achieved 43.78% under the optimized experimental conditions (co-roasting process: CG/CGCS mass ratio of 8/2, 600 °C, 1 h; H_2SO_4 leaching process: 30 wt% H_2SO_4, 90 °C, 5 h, liquid to solid ratio of 5:1 mL/g). Co-roasting induced the conversion of inert kaolinite to active metakaolinite, subsequently leading to the formation of sillimanite (Al_2SiO_5) and hercynite ($FeAl_2O_4$). The iron phases underwent a selective transformation in the following sequence: hematite (Fe_2O_3) → magnetite (Fe_3O_4) → wustite (FeO) → ferrosilite ($FeSiO_3$), hercynite ($FeAl_2O_4$), and fayalite (Fe_2SiO_4). Furthermore, we found that acid solution and leached residue both have broad application prospects. This study highlights the significant potential of co-roasting CG and CGCS for high-value utilization.

Keywords: co-roasting; H_2SO_4 leaching; phase transformation; Al; Fe extraction

check for updates

Citation: Zhao, J.; Yu, T.; Zhang, H.; Zhang, Y.; Ma, L.; Li, J.; Qu, C.; Wang, T. Study on Extraction Valuable Metal Elements by Co-Roasting Coal Gangue with Coal Gasification Coarse Slag. *Molecules* **2024**, *29*, 130. https://doi.org/10.3390/molecules29010130

Academic Editor: Giuseppe Arena

Received: 3 October 2023
Revised: 13 December 2023
Accepted: 19 December 2023
Published: 25 December 2023

Copyright: © 2023 by the authors. Licensee MDPI, Basel, Switzerland. This article is an open access article distributed under the terms and conditions of the Creative Commons Attribution (CC BY) license (https://creativecommons.org/licenses/by/4.0/).

1. Introduction

Coal gangue (CG) is a solid waste generated in the process of coal mining and washing, constituting approximately 10–15% of the total coal production [1,2]. Currently, China's coal gangue reserves amount to around 7 billion tons, with its production continuously increasing each year, making it one of the largest industrial wastes [3,4]. Coal gasification slag (CGS) is a solid waste generated by the coal gasification process. It primarily consists of residual materials derived from raw coal, which undergo a series of processes including crushing, melting, sintering, gasification, deposition, and accumulation. Ultimately, CGS comprises residues that have not undergone redox and gasification reactions. Depending on the particle size, it can be further classified into two categories: coal gasification coarse slag (CGCS) and coal gasification fine slag (CGFS) [5]. The coal gasification process consumes approximately 100 million tons of coal annually, with the national production of CGS exceeding 60 million tons per year and showing exponential growth [6]. The deposition of CG and CGS typically occurs in open piles on vacant land. Despite the distance from urban areas, the accumulation of substantial quantities of coal-based waste residues still engrosses significant land resources and poses a grave ecological threat. The environmental concerns

encompass air pollution caused by dust, water pollution, and soil contamination from heavy metals (Cu, Cd, Cr, Pb, Zn, Hg, and Sn), as well as various geological hazards [7,8]. Additionally, the oxidative spontaneous combustion during stacking of CG and CGS results in the emission of detrimental gases such as CO_2, CO, H_2S, SO_2, and NO_x [9]. In addition, both CG and CGS exhibit high concentrations of silicon, aluminum, iron, and titanium. The primary constituents of CG include quartz, clay minerals, and carbonaceous materials [10]. On the other hand, the mineral composition of CGS is predominantly composed of amorphous alumino-silicates, crystalline phase minerals, and residual carbon. Amorphous alumino-silicates account for over 60% of the total composition while quartz and calcite dominate the crystalline phase minerals [11].

At present, the comprehensive utilization of CG and CGS is primarily concentrated in areas such as combustion and power generation, construction materials, fertilizers, chemical product extraction and preparation, boiler blending, and ecological restoration [12–14]. However, the comprehensive utilization rate of both CG and CGS in China significantly lags behind that of developed countries. Therefore, it is strategically imperative to undertake extensive utilization of CG and CGS. Leaching is a widely used method for metal extraction and can be performed using various types of solvents and reagents. It involves dissolving the metal from the raw material into a liquid solution, which can then be further processed to isolate the metal. Leaching represents an energy-efficient process that can be optimized to minimize waste generation and mitigate environmental impact. Nevertheless, it is crucial to consider the potential environmental consequences associated with any extraction method and opt for the most environmentally friendly alternative whenever feasible.

Currently, the main methods regarding the extraction of aluminum from coal gangue (CG) and coal gasification slag (CGS) are alkali and acid methods [15,16]. Alkali methods, including sintering and leaching [16], have been extensively studied for the extraction of alumina from CG and CGS. However, the sintering method requires high temperatures (around 1100 °C to 1200 °C), resulting in increased energy consumption and significant emission of dicalcium silicate residue [17]. In addition, the alkali leaching method enables the alumina in CG and CGS to transform into a sodium aluminate solution, while iron and titanium become insoluble residue, resulting in a waste of resources. Additionally, alkaline solutions dissolve silica in CG and CGS, necessitating an additional desilication process [18]. Consequently, the application of alkali methods for aluminum extraction is not promising.

Compared with alkali methods, acid extraction offers competitiveness and suitability for treating CG and CGS due to its advantages such as a shorter process duration, lower energy consumption, easy separation of silica and aluminum components, as well as thorough separation. Although there are fewer studies on iron extraction from CG and CGS at present time, common methods include acid leaching extraction or reductive roasting-magnetic separation. Reduction roasting-magnetic separation involves roasting under a reducing atmosphere (e.g., H_2 [19,20], methane, or natural gas [21]), which facilitates rapid conversion of hematite to magnetite in CG and CGS followed by magnetic separation to obtain magnetite. Similar to acid extraction of aluminum, acid extraction of iron also possesses these advantages. However, it should be noted that acid leaching extraction usually requires pre-activation when extracting iron and aluminum from CG and CGS.

Various methods, including mechanical activation and thermal activation (roasting activation, and microwave activation) [22–24], have been reported as effective pre-activation approaches for acid leaching to extract the available components in CG and CGS. However, a single activation method often fails to achieve efficient extraction, leading to the adoption of composite activation methods in current research for extracting its active ingredients [25,26]. Qin et al. [23] employed a combination of mechanical grinding, low-temperature roasting, and deionized water leaching to extract aluminum and other trace elements from CG. The fully ground CG was sieved through a 100-mesh sieve and mixed according to the mass ratio of CG:NH_4Cl:$(NH_4)_2SO_4$ = 1:2:1. Subsequently, the mixture was subjected to roasting at 400 °C for 1 h in a muffle furnace. The roasted sample was

placed in a conical flask of 20 mL of 0.4 m deionized water and shaken at 60 °C for 1 h. The final leaching yields of Al, Li and Fe were 56.35%, 80.83% and 32.77%, respectively. Han et al. [27] used an acid-base combination method, wherein a 2.0 mol/L KOH solution was utilized as an activator to immerse the activated CG in a hydrochloric acid solution (2.0 mol/L) for 2 h. The resulting acid leach solution was subsequently evaporated at 110 °C for 2 h, yielding extraction rates of Al^{3+} and Si^{4+} after drying that reached as high as 78.9% and 69.2%, respectively. Shao et al. [2] proposed a recovery technology using a combination of thermal activation + HNO_3 leaching to treat CG. Following milling, the CG was subjected to thermal activation at 550 °C for 0.5 h in a muffle furnace. Under optimized leaching conditions (150 °C, theoretical HNO_3 dosage, liquid-solid ratio of 5:1 mL/g, and 2 h), extraction rates of aluminum, gallium, lithium, and iron were achieved at 95.2%, 56.4%, 80.5%, and 2.1%, respectively. Additionally, flotation is also a valuable method to upgrade solid particles before leaching [28,29], which can not only improve the efficiency and quality of aluminum and iron extraction by acid leaching, but also minimizes the process cost and environmental pollution. Moreover, it finds extensive application in the efficient recovery of minerals, solid waste, as well as heavy metal ions present in water.

In these methods, the leaching rate of valuable metal elements is influenced not only by process conditions but also by the composition of CG and CGS. These existing techniques are difficult to directly replicate and apply. Furthermore, most studies focus on single coal-based waste residues such as CG, CGS, and fly ash, with limited research on extracting valuable metal elements from two or more coal-based waste residues. Therefore, it is necessary to explore a leaching process condition that can simultaneously extract valuable metal elements from both CG and CGS. It should be noted that both CG and CGCS contain fixed carbon which can act as a reducing agent during the reduction roasting process. Based on current research progress, an innovative approach involving co-roasting and H_2SO_4 leaching was proposed for extracting valuable metal elements (Al, Fe) from CG and CGCS. This study addresses the gap in synergistic extraction of valuable metal elements from both CG and CGCS; compared to separate extraction methods, it improves the leaching rate of valuable metal elements while reducing energy consumption and H_2SO_4 dosage. The aim of this method is to provide technical support for achieving synergistic extraction of valuable metal elements from two or more coal-based waste residues.

2. Results and Discussion

2.1. Optimization of Co-Roasting Parameter

The influence of CGCS content on the extraction efficiency of valuable metal elements was investigated by thoroughly mixing CG with CGCS in a specific ratio, followed by flat placement in a corundum crucible and co-roasting in a tubular pyrolysis furnace at 700 °C for 1 h. Simultaneously, the leaching conditions were set as follows: leaching temperature of 50 °C, H_2SO_4 concentration of 30 wt%, liquid to solid ratio of 5:1 mL/g, and leaching time of 5 h.

As depicted in Figure 1a, in the absence of CGCS addition, the leaching rates of Al^{3+} and TFe were merely 23.74% and 57.22%, respectively. With an increase in CGCS content, the leaching of Al^{3+} exhibited a non-linear trend with an initial decrease followed by an increase before declining again, reaching its peak at 32.69% for a content of 20 wt%. Conversely, the leaching rate of TFe gradually increased and reached its maximum value of 69.52% when the CGCS content was at 25 wt%. This behavior can be attributed to the lower percentage of Al^{3+} content compared to that of TFe within CGCS, resulting in an enhanced release of TFe as more CGCS is added. Additionally, the decrease in the extraction rate of Al^{3+} can be attributed to the relatively low initial Al content in the CGCS sample compared to CG. As the amount of CGCS added increases, there is a gradual reduction in the overall Al content in the mixed raw material, ultimately leading to a decline in the extraction rate of Al^{3+}. Furthermore, there was a notable rise in carbon content which facilitated sufficient CO generation for hematite (Fe_2O_3) reduction. Considering both the high proportion of

CG present in the co-roasting mixture and elevated aluminum concentration within CG itself, it was deemed appropriate to select a CGCS addition level at 20 wt%.

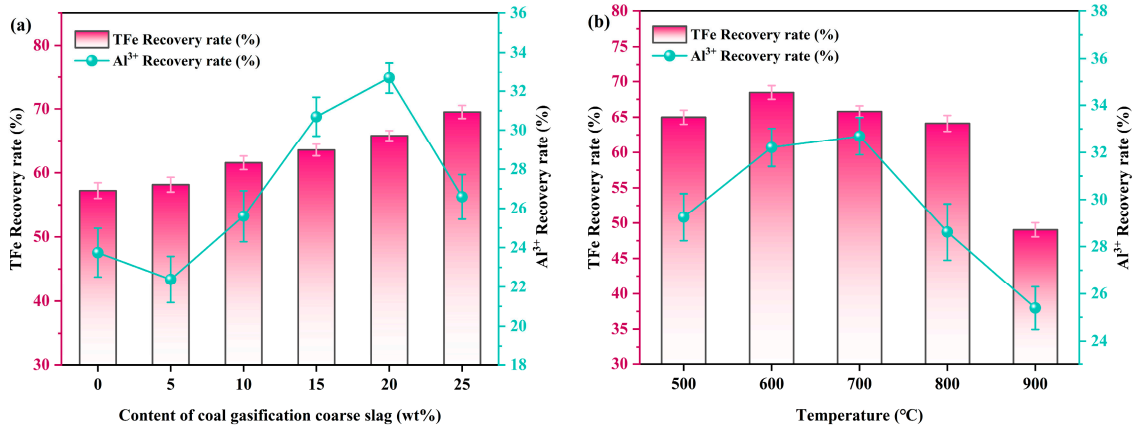

Figure 1. (**a**) The effect of different CGCS content on the leaching rates of Al^{3+} and TFe, (**b**) the effect of different co-roasting temperature on the leaching rates of Al^{3+} and TFe (co-roasting process: 1 h; H_2SO_4 leaching process: 30 wt% H_2SO_4, 50 °C, 5 h, liquid to solid ratio of 5:1 mL/g).

As shown in Figure 1b, the effect of co-roasting temperature on the extraction of valuable metal elements was investigated by incorporating 20 wt% CGCS, while keeping other conditions such as liquid to solid ratio constant. With the increase in co-roasting temperature, the leaching rates of Al^{3+} and TFe initially exhibited an upward trend followed by a decline. At 600 °C, the leaching rate of TFe reached a peak of 68.47%, indicating that the reduction effect of co-roasting was optimized at this time. This can be attributed to the temperature-induced promotion of hematite (Fe_2O_3) reduction to magnetite (Fe_3O_4) and wustite (FeO). However, as the temperature continued to rise, the leaching rate of TFe gradually decreased due to potential formation of other substances that hindered iron phase reduction in the co-roasting process. The leaching rates of Al^{3+} were measured at 32.21% and 32.69% at temperatures of 600 °C and 700 °C, respectively, which could be attributed to metakaolinite becoming inert material beyond 700 °C resulting in minimal or even negative impact on leaching rates' enhancement. Therefore, considering both leaching rates' performance and economic factors, a co-roasting temperature of 600 °C was selected.

2.2. Raw Material Characterization

The XRD pattern of CG raw material and mixed raw material are presented in Figure 2a, revealing predominant mineral constituents including kaolinite, quartz, hematite, muscovite, and calcite. Figure 2b displays the FTIR spectra of CG raw material and mixed raw material. The bands observed at 914, 3620 cm^{-1} and 3653, 3678, 3693 cm^{-1} can be attributed to the internal and external OH stretching vibrations in the layered structure of kaolinite octahedron [30,31]. Additionally, characteristic bands corresponding to Al-O-Si and Al-O vibrations in kaolinite were identified at 534 and 692 cm^{-1}, respectively [32,33]. Furthermore, absorption peaks at 428 and 1114 cm^{-1} along with double peaks at 1029 and 1006 cm^{-1} correspond to the Si-O vibration in kaolinite. Lastly, absorption peaks observed at 796 and 752 cm^{-1} are indicative of the Si-O-Si stretching vibration in kaolinite [34,35].

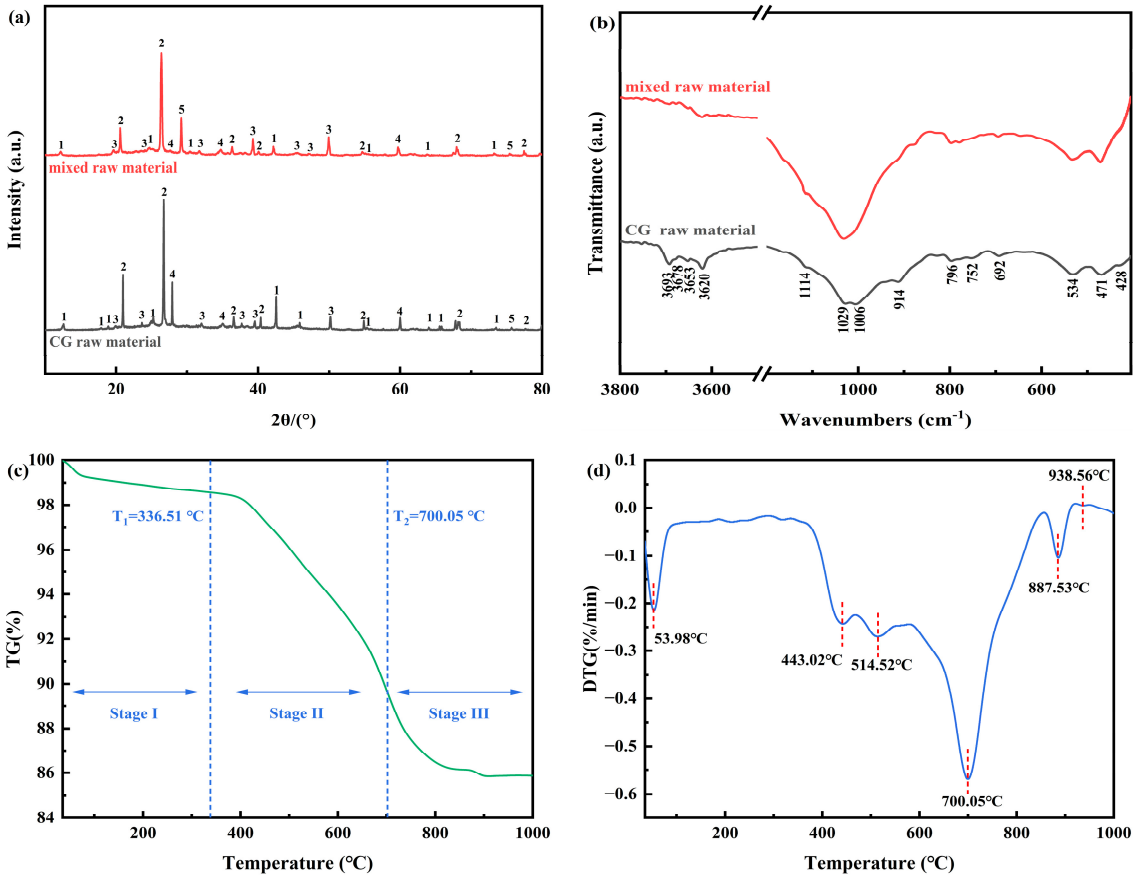

Figure 2. (**a**) XRD patterns of CG raw material, mixed raw material; 1—kaolinite; 2—quartz; 3—hematite; 4—muscovite; 5—calcite; (**b**) FTIR spectra of CG raw material and mixed raw material, (**c**,**d**) TG and DTG curves of co-roasting process.

The co-roasting of coal gangue and coal gasification coarse slag was divided into three stages based on the variations in TG and DTG curves, as shown in Figure 2c,d. Stage I occurred at an onset temperature of 35 °C–336.51 °C, accompanied by moisture evaporation. Stage II, ranging from 336.51 °C to 700.05 °C, involved the release of volatiles, carbon burning, and observed structural hydroxyl desorption of kaolinite [31,36]. This stage exhibited a maximum DTG peak with a value of 0.569%/min at a corresponding temperature of 700.05 °C. Stage III existed within the range of 700.05 °C–1000 °C and displayed two DTG peaks at temperatures of 887.53 °C and 938.56 °C, respectively; this finding may be attributed to macromolecular organic matter degradation, fixed carbon decomposition, and mullite formation [37].

2.3. Phase Transformation during Co-Roasting Process

The XRD patterns of the co-roasting products obtained at different co-roasting temperatures are presented in Figure 3a. At 500 °C, the diffraction peaks of kaolinite still persist but with reduced intensity compared to the mixed raw material, indicating partial decomposition of kaolinite [38]. Upon increasing the temperature from 500 °C to 600 °C, the diffraction peaks of kaolinite disappear completely, suggesting successful transformation from inert kaolinite to active metakaolinite. Notably, active metakaolinite appears amorphous and does not exhibit any discernible features in XRD analysis [39]. Additionally, some hematite diffraction peaks vanish at 500 °C while a new magnetite phase is detected.

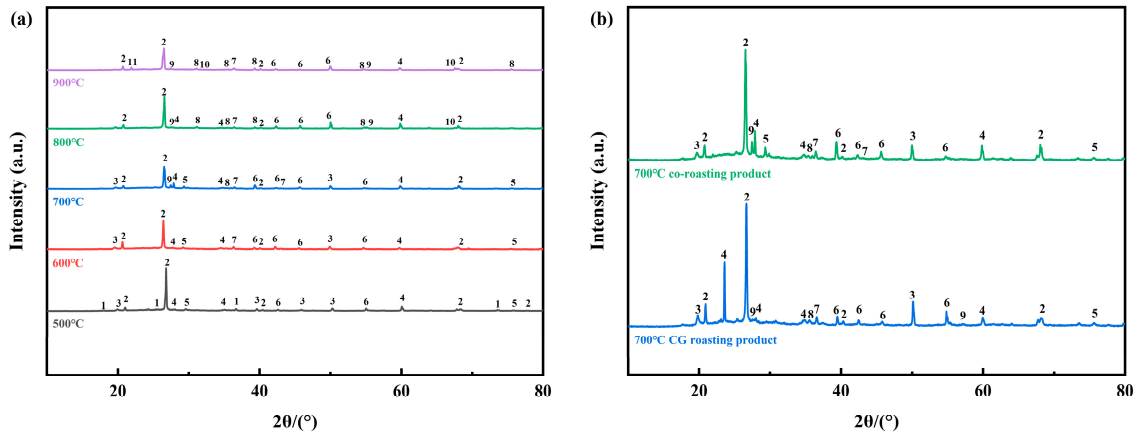

Figure 3. (**a**) XRD patterns of 500 °C–900 °C co-roasting products; (**b**) XRD patterns of 700 °C CG roasting product, 700 °C co-roasting products; 1—kaolinite; 2—quartz; 3—hematite; 4—muscovite; 5—calcite; 6—magnetite; 7—wustite; 8—fayalite; 9—sillimanite; 10—hercynite; 11—ferrosilite.

Further increasing temperature to 600 °C, a significant decomposition of hematite occurred, leading to an increase in the diffraction peaks of magnetite. Meanwhile, the presence of wustite was observed following co-roasting at 600 °C. Subsequently, at temperatures ranging from 700 °C–900 °C, distinct diffraction peaks corresponding to fayalite, sillimanite, hercynite, and ferrosilite were identified [40–43]. This observation elucidates why the reduction of iron phases during co-roasting was impeded and resulted in a minimal or even decreased leaching rate of Al^{3+}. Notably, at a co-roasting temperature of 800 °C, calcite underwent decomposition while muscovite remained remarkably stable even when subjected to elevated temperatures up to 900 °C.

Figure 3b displays the XRD patterns of the CG roasting product and co-roasting product at 700 °C. As depicted in the figure, compared to the solely CG roasting product at 700 °C, the diffraction peaks of hematite are weaker while those of magnetite are stronger in the co-roasting product at 700 °C, and there is an increase in wustite's number of diffraction peaks. This can be attributed to a higher carbon content in mixed raw material that provides a better reducing atmosphere and promotes further reduction of iron phases [44,45]. Additionally, there are more diffraction peaks for sillimanite in CG roasting products than co-roasting products which result in a lower leaching rate for Al^{3+}.

The aforementioned results demonstrate that the temperature increase and carbon presence contribute to the reduction of iron phase in the co-roasting process. However, excessively high temperatures lead to sintering of wustite with Si and Al in the mixed raw material, resulting in the formation of other iron phases which impede iron phase reduction. Simultaneously, as temperature increases, metakaolinite reacts with Si and Fe in the mixed raw material to form sillimanite and hercynite, consequently reducing the leaching rate of Al^{3+}.

The co-roasting products were characterized using FTIR analysis. As depicted in Figure 4, at a co-roasting temperature of 500 °C, the gradual removal of the hydroxyl group from kaolinite resulted in the absence of absorption peaks associated with OH stretching vibrations (3693, 3678, 3653, 3620, and 914 cm^{-1}), indicating the initiation of kaolinite transformation into metakaolinite [18,31]. Simultaneously, a decrease in the intensity of Al-O-Si stretching vibration at 534 cm^{-1} suggested that the dehydroxylation process was accompanied by the disruption of Al-O-Si bonds and exacerbation of crystal defects.

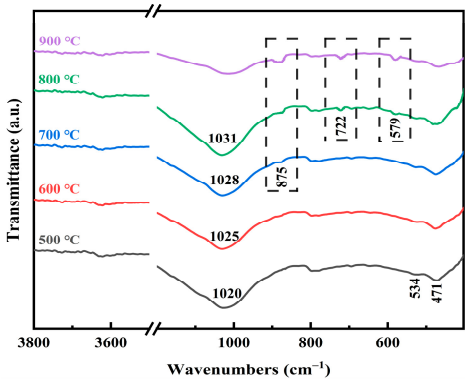

Figure 4. FTIR patterns of 500 °C–900 °C co-roasting product.

With the further increase in co-roasting temperature, the Si-O vibration peaks at 1006 and 1029 cm^{-1} merge into a broadband peak at 1020 cm^{-1}, which subsequently shifts to shorter wavelengths between 500 °C–800 °C. This shift is attributed to the enhanced orderliness of the silicate structure [45]. During the transformation of kaolinite into metakaolinite, as metakaolinite gradually loses its ordering and average bond angle increases within the Si-O-Si network, the stretching vibration peak at 471 cm^{-1} assigned to Si-O-Si weakens and broadens with increasing temperatures from 500 °C–800 °C [46].

Significantly, the adsorption bond located at 875 cm^{-1} associated with inert sillimanite (Al_2SiO_5) was detected after co-roasting at temperatures ranging from 700 °C to 900 °C [45]. Furthermore, the characteristic peaks of hercynite ($FeAl_2O_4$) related to Fe-O at 579 cm^{-1} and Al-O bond at 722 cm^{-1} were observed after co-roasting within the temperature range of 800 °C–900 °C [47]. These findings are consistent with the XRD results, providing further evidence for the formation of new inert components contributing to the decrease in leaching rates of Al^{3+} and TFe.

In addition to XRD and FTIR, XPS analysis was conducted to characterize the mixed raw material and co-roasting products. The effect of co-roasting on the atomic valence characteristics of mineral surfaces was investigated through XPS analysis in Figure 5. Figure 5a illustrates the comprehensive survey scans of the six samples, revealing that Si, Al, Fe, O, C, K, Ca, Mg, and Na were the predominant elements at the surface. These findings align with the chemical composition and proximate analysis of raw materials.

In Figure 5b, the high-resolution XPS survey of Fe2p for these six samples reveals that the Fe2p3/2 peak exhibits a narrower width, higher intensity, and larger area compared to the Fe2p1/2 peak due to spin-orbit (j-j) coupling [48–50]. The Fe2p spectrum of the mixed raw material indicates that the two photoelectron peaks at binding energies of 726.9 eV (Fe2p1/2) and 712.79 eV (Fe2p3/2) can be attributed to Fe^{3+}, which appears to correspond with the presence of Fe^{3+} in the hematite phase [51,52]. Additionally, the observed photoelectron peaks related to Fe(II) minerals in trace amounts seem to represent contributions from Fe^{2+} species.

According to Figure 5b, the Fe^{2+} content of the co-roasting product at 500 °C exhibited an increase, with the ratio of Fe^{2+}/Fe^{3+} rising from 1.06 to 1.12. Additionally, lower binding energy revealed a low intensity peak of Fe^{2+}, indicating the transformation of hematite after co-roasting and contributing to the presence of magnetite in the product at 500 °C [51,53]. This suggests that reduction from the Fe^{3+} state to Fe^{2+} has occurred [54]. Moreover, these findings align with those obtained from XRD analysis as evidenced by satellite peaks (714.98 eV and 729.18 eV) observed in the co-roasting product at 600 °C for Fe^{2+}. The ratio of Fe^{2+}/Fe^{3+} further increased to 1.18 during this stage. Since magnetite does not exhibit satellite peaks [49,55], it can be inferred that these satellite peaks are attributed to wustite based on XRD analysis results, signifying that the transition from magnetite to wustite has already taken place. Specifically, with the increase in co-roasting temperature, the binding energy positions of the maxima of the Fe2p3/2 and Fe2p1/2 peaks were shifted from 710.4 eV and 724.2 eV to 709.72 eV and 723.32 eV, with negative shifts of 0.68 eV

and 0.88 eV, respectively, compared to the mixed raw material. Moreover, there was an increase in the Fe^{2+}/Fe^{3+} ratio to 2.43, indicating a change in the chemical environment where more divalent iron is present (i.e., alterations in types and quantities of elements bound to it [56]). Combining these findings with XRD analyses, it can be attributed that within the co-roasting product at temperatures ranging from 700 °C–900 °C, Fe^{2+} originates from two sources: a minor contribution from magnetite formation and transformation of wustite into fayalite, hercynite, and ferrosilite phases.

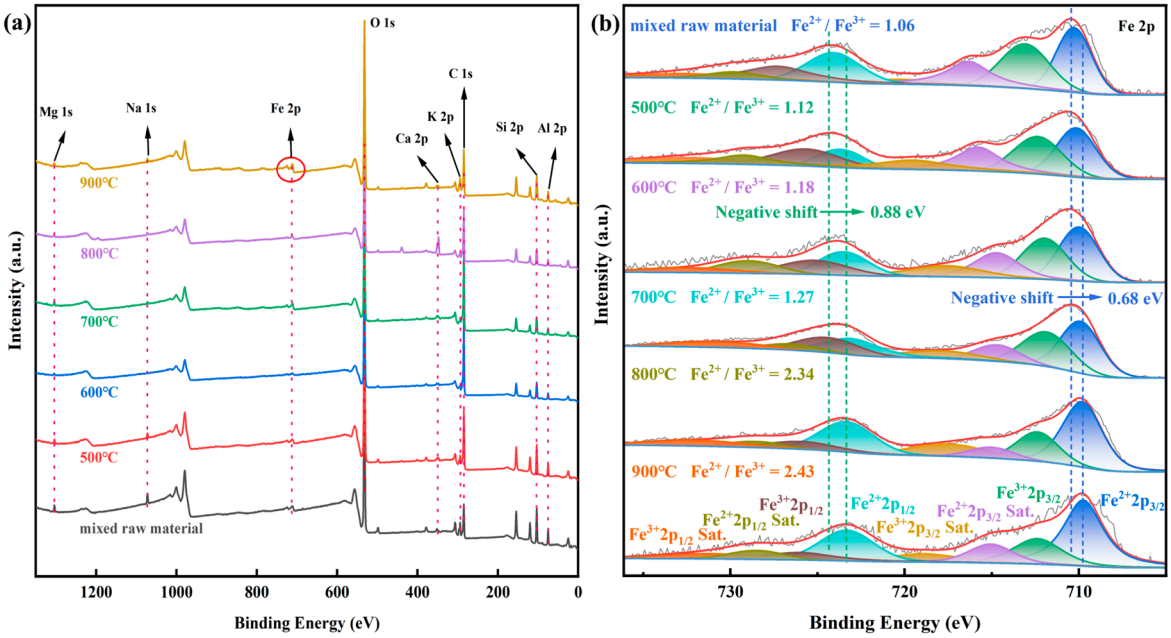

Figure 5. XPS analysis (**a**) survey scan XPS spectra for mixed raw material, and 500 °C–900 °C co-roasting products; XPS survey of Fe2p for (**b**) mixed raw material, and 500 °C–900 °C co-roasting products.

The XPS results mentioned above provide robust evidence supporting the transformation of hematite phase into magnetite, wustite, fayalite, hercynite, and ferrosilite phases during the co-roasting process. Additionally, this phase transformation process resulted in a reduction in both TFe and Al^{3+} leaching rates.

2.4. Co-Roasting Reaction Mechanism

The reactions that may occur during the co-roasting process of mixed raw material are enumerated as Equations (1)–(11) [57,58]. Thermodynamic calculations for some of the reactions were performed using HSC 9.0 software, and the temperature dependency of $\Delta_r G^\theta$ is illustrated in Figure 6.

$$3Fe_2O_3\ (s) + C\ (s) \rightarrow 2Fe_3O_4\ (s) + CO\ (g) \quad (1)$$

$$3Fe_2O_3\ (s) + CO\ (g) \rightarrow 2Fe_3O_4\ (s) + CO_2\ (g) \quad (2)$$

$$6Fe_2O_3\ (s) + C\ (s) \rightarrow 4Fe_3O_4\ (s) + CO_2\ (g) \quad (3)$$

$$Fe_3O_4\ (s) + C\ (s) \rightarrow 3FeO\ (s) + CO\ (g) \quad (4)$$

$$Fe_3O_4\ (s) + CO\ (g) \rightarrow 3FeO\ (s) + CO_2\ (g) \quad (5)$$

$$FeO\ (s) + Al_2O_3\ (s) \rightarrow FeAl_2O_4(s) \quad (6)$$

$$FeO\ (s) + SiO_2\ (s) \rightarrow FeSiO_3(s) \quad (7)$$

$$2FeO\ (s) + SiO_2\ (s) \rightarrow Fe_2SiO_4(s) \quad (8)$$

$$Al_2O_3{\cdot}2SiO_2{\cdot}2H_2O\ (s) \rightarrow Al_2O_3{\cdot}2SiO_2\ (s) + 2H_2O\ (g) \quad (9)$$

$$Al_2O_3{\cdot}2SiO_2(s) + 0.5Fe_2O_3(s) + 0.5C\ (s) \rightarrow FeAl_2O_4(s) + 2SiO_2(s) + 0.5CO\ (g) \quad (10)$$

$$2[Al_2O_3{\cdot}2SiO_2]\ (s) \rightarrow 0.5Al_2SiO_5(s) + 1.5SiO_2\ (s) + [Al_2O_3{\cdot}2SiO_2]\ (s) + 0.5[\gamma - Al_2O_3]\ (s) \quad (11)$$

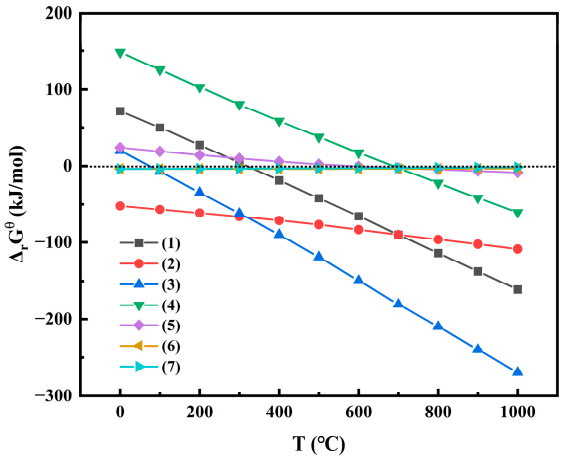

Figure 6. Diagram of Gibbs free energy ($\Delta_r G^\theta$) versus temperature for reactions occurring during the co-roasting process of mixed raw material.

Due to the unavailability of data on metakaolinite, the phase transformation temperature of kaolinite during thermal activation is inferred from experimental findings reported by literature [59,60]. The transition temperature from kaolinite to metakaolinite ranges between 500 °C and 700 °C [Equation (9)].

The diagram in Figure 7 illustrates the mechanism of co-roasting CG and CGCS. During the co-roasting process, hematite (Fe_2O_3) is reduced to magnetite (Fe_3O_4), which further undergoes reduction to wustite (FeO) due to the presence of fixed carbon in CG and CGCS. Subsequently, wustite (FeO) reacts with Si and Al elements in the mixed raw material, resulting in the formation of iron phases such as ferrosilite ($FeSiO_3$), hercynite ($FeAl_2O_4$), and fayalite (Fe_2SiO_4). Additionally, kaolinite present in the mixed raw material undergoes dehydration into metakaolinite, which then transforms into sillimanite (Al_2SiO_5) and hercynite ($FeAl_2O_4$). In summary, CGCS enables efficient reduction of iron minerals in CG while also enhancing leaching rates of Al^{3+} and TFe.

2.5. Optimization of H_2SO_4 Leaching Parameter

After conducting the co-roasting experiment, a significant enhancement in the activity of aluminum and iron was observed. Consequently, batch experiments were conducted to investigate the optimal leaching conditions, encompassing H_2SO_4 concentration and leaching temperature.

As can be seen from Figure 8a, the effect of H_2SO_4 concentration (10–50 wt%) on the extraction of valuable metal elements were investigated under this conditions, including a CGCS content of 20 wt%, co-roasting in a tubular pyrolysis furnace at 600 °C for 1 h, leaching temperature of 50 °C, liquid to solid ratio of 5:1 mL/g, and leaching time of 5 h. With the increase in H_2SO_4 concentration, the leaching rates of Al^{3+} and TFe exhibited an initial upward trend followed by a plateau. Specifically, at an H_2SO_4 concentration of 30 wt%, the leaching rate of TFe was measured to be 68.47%, while that of Al^{3+} was found to be 32.21%. Subsequently, further increases in H_2SO_4 concentration only resulted in marginal changes in the leaching rates of Al^{3+} and TFe, indicating near-complete reaction between Al^{3+}, TFe, and H_2SO_4 at a concentration of 30 wt%. Therefore, it can be inferred that co-roasting pretreatment with CG and CGCS achieves optimal leaching efficiency when using an H_2SO_4 concentration of 30 wt%.

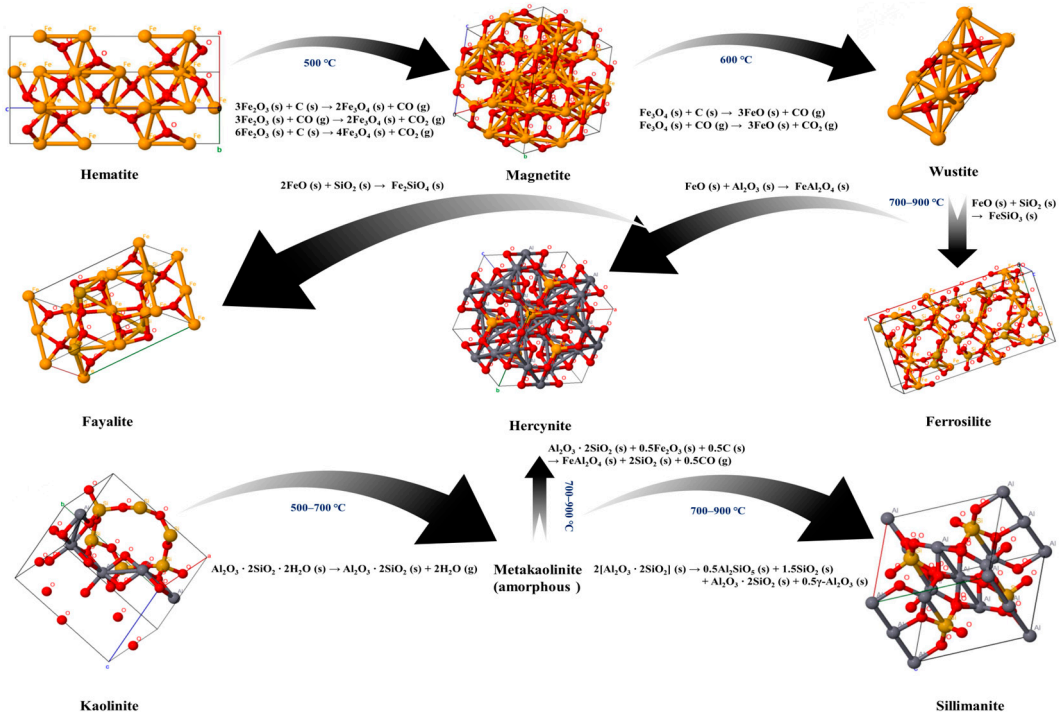

Figure 7. Mechanism of co-roasting of CG and CGCS.

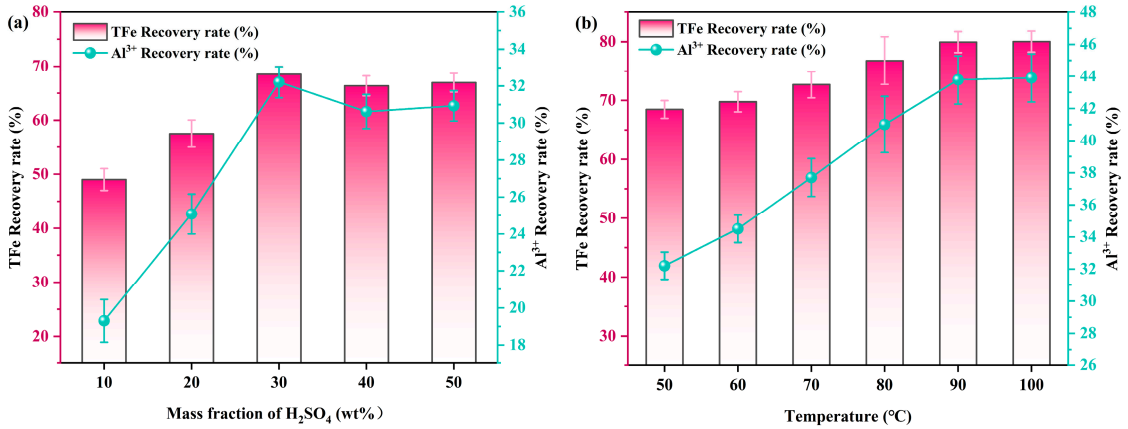

Figure 8. (**a**) The effect of H_2SO_4 concentration on the leaching rates of Al^{3+} and TFe, (**b**) the effect of leaching temperature on the leaching rates of Al^{3+} and TFe (co-roasting process: CG/CGCS mass ratio of 8/2, 600 °C, 1 h; H_2SO_4 leaching process: 5 h, liquid to solid ratio of 5:1 mL/g).

The effect of leaching temperature (50 °C–100 °C) on the extraction of valuable metal elements were investigated, as depicted in Figure 8b. In this study, the H_2SO_4 concentration was fixed at 30 wt%, while other conditions such as the liquid to solid ratio were maintained constant. As shown in Figure 8b, the leaching rates of Al^{3+} and TFe at 50 °C were only 32.21% and 68.47%, respectively. As the temperature increased, both the leaching rates of Al^{3+} and TFe gradually improved; when the temperature reached 90 °C, the leaching rate of TFe reached 79.93%, while that of Al^{3+} was recorded as 43.78%. This can be attributed to enhanced diffusion processes and chemical reaction rates with increasing temperature, leading to more complete reactions. Moreover, beyond a temperature of 90 °C, further increases had minimal impact on enhancing the leaching rates of Al^{3+} and TFe significantly. Therefore, a leaching temperature of 90 °C was selected.

2.6. Analysis of Mixed Raw Material, Co-Roasting Product and Leached Residue

The mixed raw material, as well as the co-roasting product and leached residue obtained under optimal conditions, were characterized to analyze their differences. The SEM-EDS images of the three samples are recorded and presented in Figure 9. As depicted in Figure 9a, the particle size distribution of the mixed raw material exhibits non-uniformity, while displaying a typical lamellar structure of kaolinite. In Figure 9b, it can be observed that despite dehydroxylation of kaolinite into metakaolinite during co-roasting, the lamellar structure still exists, which may be attributed to the fact that although the $AlO_2(OH)_4$ octahedral layer is damaged, the SiO_4 tetrahedral layer can still maintain the lamellar structure. Furthermore, Figure 9c presents a scanning electron microscope image of the leached residue revealing evident signs of erosion. This indicates that after leaching aluminum and iron with sulfuric acid, the microstructure of aluminosilicates is disrupted. Additionally, both co-roasting product and leached residue exhibit some pore structures.

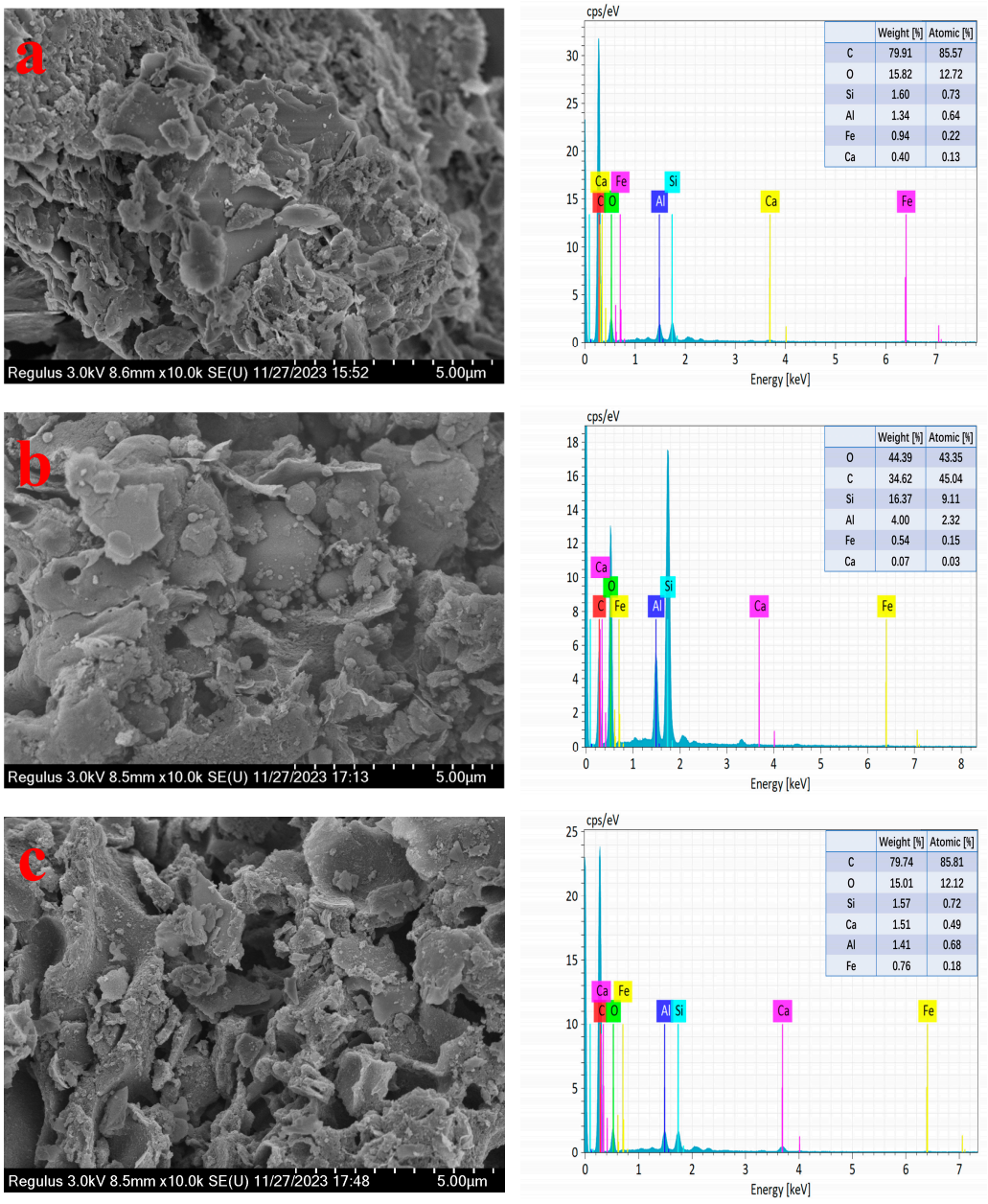

Figure 9. SEM and EDS images of mixed raw material (**a**), co-roasting product (**b**), and leached residue (**c**).

The EDS diagram in Figure 9 reveals a significantly higher mass percentage of elemental Ca in the leached residue compared to the other two samples, which may be due to the reaction of sulphuric acid with CaO in the samples to generate calcium sulphate, resulting in the enrichment of calcium ions in the leached residue.

The particle size distribution of the mixed raw material, co-roasting product, and leached residue is illustrated in Figure 10. The average particle sizes of the mixed raw material, co-roasting product, and leached residue were determined to be 151.10 μm, 103.87 μm, and 42.86 μm, respectively. Notably, the leached residue exhibited the smallest average particle size among all samples investigated, consistent with SEM observations and further confirming its abundant pore structure.

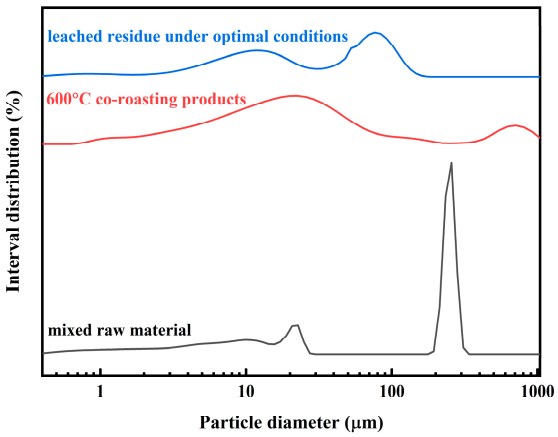

Figure 10. The particle size distribution of the mixed raw material, co-roasting product, and leached residue.

2.7. Prospects and Challenges in the Application of Acid Solution and Leached Residue

Table 1 illustrates the Chemical composition (wt%) of leached residue and chemical content (g/L) of an acid solution. As given in Table 1, alumina, potassium oxide, iron oxide and sodium oxide from the co-roasting product were partially dissolved in the acid solution, while calcium oxide and magnesium oxide reacted with sulphuric acid and were deposited in the leached residue, and the leached residue had the largest percentage of SiO_2; this is in agreement with the results of XRD analyses (Figure S3) of the leached residue.

Table 1. Chemical composition (wt%) of leached residue and chemical content (g/L) of an acid solution.

	SiO_2	**Al_2O_3**	**K_2O**	**Fe (Fe_2O_3, Fe_3O_4, FeO, etc.)**	**S ($CaSO_4$, $MgSO_4$, etc.)**	**Na_2O**	**Others**
The chemical composition (wt%) of leached residue	74.29	13.44	3.31	1.34	0.524	0.492	6.604
	$Al_2(SO_4)_3$		$FeSO_4$	$Fe_2(SO_4)_3$	K_2SO_4	Na_2SO_4	Others
The chemical content (g/L) of an acid solution	0.82		0.92	0.09	0.02	0.01	<0.01

Most of the existing coal-based waste treatment technologies focus solely on extracting valuable metal elements from a single type of coal-based waste residue, neglecting the synergistic extraction potential of multiple types of coal-based waste residues. In this study, a combination of CG and CGCS co-roasting + H_2SO_4 leaching was employed to extract valuable components (Al, Fe) from the acid solution, resulting in a leached residue with high silicon content and abundant pore structures. This indicates that both the acid solution and leached residue obtained in this study possess rich usable resources; however,

effectively harnessing their value while minimizing environmental pollution remains a significant challenge. The technologies for disposal of coal-based waste residues have been systematically summarized and compared, with results presented in Table 2.

Table 2. Summary and comparison of coal-based waste residues disposal technologies.

Substance	Methods	Reagents	Extraction	Application	Ref.
Acid solution (high-iron CG)	Calcination + acid leaching	HCl	Al: 90% Fe: 91%	Preparation of PAFC flocculants	[61]
Acid solution (high-alumina fly ash)	Acid leaching + direct-electricity conversion technology + roasting	HCl	No reported	Preparation of Al_2O_3	[62]
Aacid solution (coal-bearing kaolinite)	Mechanical grinding + acid leaching	H_2SO_4	Al: 100%	Preparation of γ-Al_2O_3 powder	[63]
Leached residue (CG)	Calcination + acid leaching	HCl	No reported	Preparation of NaA zeolite	[64]
Leached residue (CGFS)	Calcination + acid leaching	HCl	The total leaching rate of all metal oxides: 80%	Preparation of mesoporous silica	[65]
Leached residue (CGS)	Non-hydrothermal sol–gel method	No reported	No reported	Preparation of MCM-41	[66]
Acid solution and leached residue (CG)	High temperature acid leaching	HCl	Al: 92.54% SiO_2: 96.01%	Preparation of Al_2O_3 and SiC	[15]
Acid solution and leached residue (CG and CGCS)	Co-roasting + acid leaching	H_2SO_4	Al: 43.78% Fe: 79.93%	Preparation of aluminium-iron flocculants and mesoporous silica	This work

We believe that the findings of these studies highlight the potential applications and benefits of utilizing H_2SO_4 acid solution and coal-based waste leached residue, providing technical support for the proper handling of acid solution and leached residue. It is crucial to note that adherence to regulations and guidelines is essential in handling these leaching wastes to minimize their environmental impact. Furthermore, our next step involves utilizing aluminum and iron ions present in the acid solution for fabricating coal-based waste residues-based aluminum-iron flocculants, which can be applied in treating industrial wastewater such as coal slurry water and dye wastewater, with a view to achieving the purpose of treating wastes with wastes. Simultaneously, we also focus on preparing mesoporous materials from acid-leached residue, with subsequent systematic investigations planned.

3. Materials and Methods

3.1. Materials

The CG and CGCS used in this study were obtained from Yan'an City, Shaanxi Province, China. The CG and CGCS were crushed and then ground with a rod mill for 2–3 min, passing through a 100-mesh sieve. The used H_2SO_4 was of analytical reagent and was purchased from Xi 'an Jiuheng Huaye Equipment Co., Ltd. The experiments were conducted using deionized water.

The chemical compositions of CG and CGCS, as well as their proximate analysis, are presented in Table 3.

Table 3. Chemical composition and proximate analysis of CG and CGCS (mass, %).

	Substance	SiO_2	Al_2O_3	Fe_2O_3	K_2O	MgO	CaO	Others	LOI
Chemical composition	Content in CG	58.02	20.87	10.67	4.41	2.17	1.34	2.52	20.10
	Content in CGCS	28.80	10.51	20.23	1.37	2.36	31.93	4.80	36.75
	Substance	Moisture		Ash		Volatiles		Fixed carbon	
Proximate analysis	Content in CG	1.7		85.81		9.93		2.56	
	Content in CGCS	2.15		74.88		5.78		17.19	

The Sulphur content of CG and CGCS both are <0.1%.

3.2. Experimental Procedures

The schematic in Figure 11 illustrates the co-roasting experiment of CG and CGCS, consisting of two main steps: co-roasting and H_2SO_4 leaching. In a typical co-roasting experiment, the as-received CG was thoroughly mixed with CGCS in a specific ratio, placed flat in a corundum crucible, and subjected to co-roasting at predetermined temperatures (500 °C–900 °C) and duration (1 h) using a tubular pyrolysis furnace (model GSL-1500X). The tubular pyrolysis furnace is filled with N_2 gas to provide a reduced atmosphere. To investigate the effect of co-roasting+H_2SO_4 leaching conditions on the extraction efficiency of valuable metal elements, the leaching process was conducted under the following conditions: leaching temperatures ranging from 50 °C to 100 °C, H_2SO_4 concentration varying from 10 wt% to 50 wt%, liquid to solid ratio set at 5:1 mL/g, and a leaching time of 5 h. The optimization process of the above experimental conditions is shown in Figures S1 and S2. The co-roasting product was subjected to H_2SO_4 leaching in a flat-bottomed flask equipped with a condensing device.

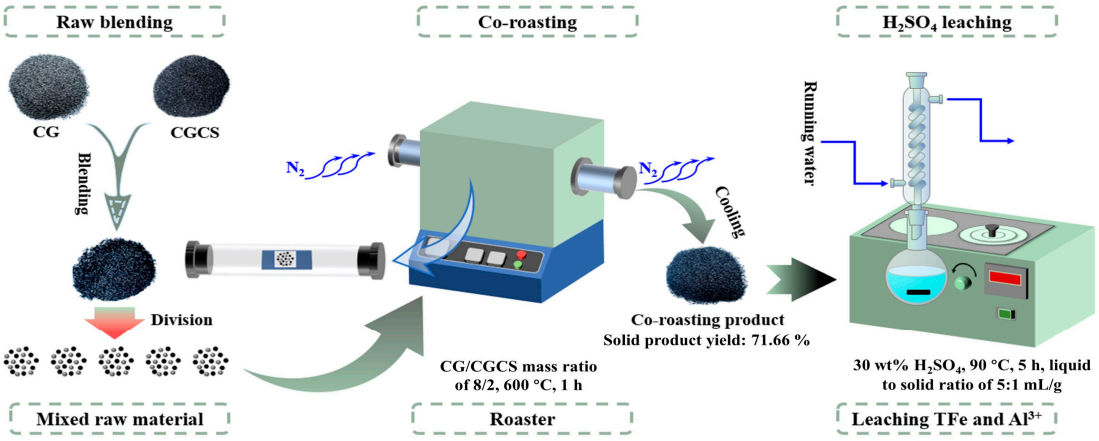

Figure 11. Schematic of CG and CGCS co-roasting experiment.

Firstly, the co-roasting product obtained under optimal co-roasting conditions was mixed with predetermined amounts of H_2SO_4 at a specified liquid to solid ratio. Subsequently, the resulting slurry was transferred to a flat-bottomed flask equipped with a condensing device and subjected to reaction in a thermostatic magnetic water bath pot, while maintaining a stirring speed of 150 r/min. Once the temperature of the mixed slurry reaches the predetermined temperature, the timing for the reaction begins. After the reaction, the slurry is cooled to room temperature and filtered. Evaluate the concentration of Al^{3+} and total iron (TFe) in the leaching solution, determine the ratio of Al^{3+} and TFe in the leaching solution to that in the mixed raw material, and subsequently calculate the leaching efficiency. These indicators of aluminum and iron leaching rates in the leaching solution serve as performance assessment metrics for evaluating the effectiveness of the co-roasting process.

The equation for determining the leaching rate is as follows:

$$\eta_{Al^{3+}/TFe} = \frac{m}{M} \times 100\% \quad (12)$$

where η represents the recovery rates of Al^{3+} and TFe, while m and M denote the Al^{3+} and TFe contents in the leaching solution and mixed raw material, respectively.

3.3. Characterization Methods

The chemical compositions of both the CG, CGCS, and leached residue were analyzed by X-ray fluorescence (XRF, Tokyo Rigaku Co., Simultix 12, Tokyo, Japan). XRF analysis was conducted with an Rh target, Si (Li) crystal detector, and calibrated based on fundamental parameters. Proximate analysis of the CG and CGCS was performed according to GB/T 212-2008 standards [67]. The pyrolysis characteristics of CG and mixed raw material were recorded using a thermogravimetric analyzer (TGA 8000 Perkin Elmer, Waltham, MA, USA) from 35 °C to 1000 °C in a nitrogen atmosphere at a flow rate of 20 mL/min. The heating rates of 10 °C/min were set to research the pyrolysis characteristics. The mineral phase-evolution features of the samples were conducted by X-ray diffraction technique (XRD; Bruker D8 ADVANCE, Ettlingen, Germany) with Cu Kα radiation from 10° to 80° at a scan speed of 10 °/min. The chemical bonds and functional groups in the samples were analyzed through a Fourier transform infrared spectrometer (FTIR; Bruker VERTEX 70, Ettlingen, Germany) within the wavenumber range of 400–3800 cm^{-1}. XPS analysis was performed on a ULVAC Inc. spectrometer equipped (XPS, ULVAC PHI 5000 VersaProbe 4, Chigasaki, Japan) with monochromatic Al Kα radiation as an excitation source, and the analyzed area of 400 μm in diameter. Raw data obtained were processed by the XPS Peak Fits software package (version number: XPSpeak 41) to fit all spectra. A scanning electron microscope (JSM-6390A, Jeol, Tokiyo, Japan) was used to analyze the microscopic morphology and the type and percentage of elements of samples. The particle size distribution of the samples was determined using a laser particle size analyzer (EyeTech, S/N 60296, Carlton, VIC, Australia). Analysis of the composition of the leaching solution was performed by using spectrophotometry.

4. Conclusions

The present study proposes an innovative approach of co-roasting and H_2SO_4 leaching to extract valuable metal elements (Al, Fe) from CG and CGCS, aiming at their treatment. Through thermodynamic analyses and systematic experimental investigations, the following outcomes were obtained:

(1) The effects of various factors on the extraction efficiency of valuable metal elements (Al, Fe) were investigated through single factor experiments. Under optimal conditions including 20 wt% CGCS content, 600 °C co-roasting temperature for 1 h followed by leaching at 90 °C with a liquid to solid ratio of 5:1 mL/g using a H_2SO_4 concentration of 30 wt%, a TFe leaching rate of 79.93% was achieved along with an Al^{3+} leaching rate of 43.78% after a leaching time of 5 h. Furthermore, we found that acid solution and leached residue both have broad application prospects.

(2) The activation behavior and phase transformation mechanism during the co-roasting process were investigated through Gibbs free energy calculation, as well as XRD, FTIR, and XPS characterization analysis. Inert kaolinite in CG and CGCS was converted to active metakaolinite after co-roasting. The reaction of metakaolinite with Si and Al elements from the mixed raw material produced sillimanite (Al_2SiO_5) and hercynite ($FeAl_2O_4$). Hematite (Fe_2O_3) was reduced to magnetite (Fe_3O_4) and wustite (FeO) by fixed carbon in CG and CGCS. Subsequently, wustite reacted with Si and Al elements from the mixed raw material to form iron phases such as ferrosilite ($FeSiO_3$), hercynite ($FeAl_2O_4$), and fayalite (Fe_2SiO_4).

(3) Co-roasting+H_2SO_4 leaching provides a novel method for extensive utilization of CG and CGCS while also offering a new approach for treating two or more types of coal-based solid waste that can alleviate industry development's pressure on the environment.

Supplementary Materials: The following supporting information can be downloaded at: https://www.mdpi.com/article/10.3390/molecules29010130/s1, Figure S1: Coal gangue H_2SO_4 leaching experiments; Figure S2: Coal gangue calcination+H_2SO_4 leaching experiments; Figure S3: XRD patterns of leached residue; 1-kaolinite; 2-quartz; 3-hematite; 4-muscovite; 5-calcite; 6-magnetite; 7-wustite; 8-fayalite; 9-sillimanite; 10-hercynite; 11-ferrosilite; 12-magnesium sulfate; 13-calcium sulfate; 14-potassium oxide; 15-alumina oxide; 16-sodium oxide.

Author Contributions: J.Z.: data curation, investigation, and writing—original draft; H.Z. and J.L.: validation, conceptualization, and supervision; Y.Z. and T.W.: data curation, investigation, and formal analysis; L.M.: investigation, methodology, and data curation; C.Q.: project administration and funding acquisition; T.Y.: writing—review and editing, validation, and supervision. All authors have read and agreed to the published version of the manuscript.

Funding: The work was supported financially by the Shaanxi Provincial Department and Municipal Linkage Key Project: Key Technology Development and Engineering Demonstration of Coal-Based Waste Co-utilization in Extremely Thin Coal Seam (No. 2022GD-TSLD-69), the Special Program for Serving Localities of Shaanxi Provincial Department of Education: Research on Reuse Technology of Return Fluid from Oil and Gas Field Measures in North Shaanxi Region(No. 22JC054), the open subject of State Key Laboratory of Petroleum Pollution Control (PPC2019001), and the Xi'an Shiyou University Postgraduate Innovation and Practical Ability Training Project (No. YCS23113051).

Institutional Review Board Statement: Not applicable.

Informed Consent Statement: Not applicable.

Data Availability Statement: Data are contained within the article and Supplementary Materials.

Acknowledgments: The authors also thank the support of The Youth Innovation Team of Shaanxi University and the work of the Modern Analysis and Testing Center of Xi'an Shiyou University.

Conflicts of Interest: Authors J.Z., T.Y., H.Z., Y.Z., L.M., C.Q. were employed by the company Shaanxi Fuquan Environmental Protection Technology Co., Ltd. The remaining authors declare that the research was conducted in the absence of any commercial or financial relationships that could be construed as a potential conflict of interest.

References

1. Li, M.; Zhang, J.; Li, A.; Zhou, N. Reutilisation of coal gangue and fly ash as underground backfill materials for surface subsidence control. *J. Clean. Prod.* **2020**, *254*, 120113. [CrossRef]
2. Shao, S.; Ma, B.; Wang, C.; Chen, Y. Extraction of valuable components from coal gangue through thermal activation and HNO_3 leaching. *J. Ind. Eng. Chem.* **2022**, *113*, 564–574. [CrossRef]
3. Li, J.; Wang, J. Comprehensive utilization and environmental risks of coal gangue: A review. *J. Clean. Prod.* **2019**, *239*, 117946. [CrossRef]
4. Wang, H.; Fang, X.; Du, F.; Tan, B.; Zhang, L.; Li, Y.; Xu, C. Three-dimensional distribution and oxidation degree analysis of coal gangue dump fire area: A case study. *Sci. Total Environ.* **2021**, *772*, 145606. [CrossRef] [PubMed]
5. Shu, Q.; Sun, Z.; Zhu, G.; Wang, C.; Li, H.; Qi, F.; Zhang, Q.; Li, S. Highly efficient synthesis of ZSM-5 zeolite by one-step microwave using desilication solution of coal gasification coarse slag and its application to VOCs adsorption. *Process Saf. Environ. Prot.* **2022**, *167*, 173–183. [CrossRef]
6. Zhu, D.; Zuo, J.; Jiang, Y.; Zhang, J.; Zhang, J.; Wei, C. Carbon-silica mesoporous composite in situ prepared from coal gasification fine slag by acid leaching method and its application in nitrate removing. *Sci. Total Environ.* **2020**, *707*, 136102. [CrossRef] [PubMed]
7. Li, M.; Li, A.; Zhang, J.; Huang, Y.; Li, J. Effects of particle sizes on compressive deformation and particle breakage of gangue used for coal mine goaf backfill. *Powder Technol.* **2020**, *360*, 493–502. [CrossRef]
8. Mjonono, D.; Harrison, S.; Kotsiopoulos, A. Supplementing structural integrity of waste rock piles through improved packing protocols to aid acid rock drainage prevention strategies. *Miner. Eng.* **2019**, *135*, 13–20. [CrossRef]

9. Wu, Y.; Yu, X.; Hu, S.; Shao, H.; Liao, Q.; Fan, Y. Experimental study of the effects of stacking modes on the spontaneous combustion of coal gangue. *Process Saf. Environ. Prot.* **2019**, *123*, 39–47. [CrossRef]
10. Shi, S.; Ma, B.; Zhao, D.; Li, X.; Shao, S.; Wang, C.; Chen, Y. Thermal Behavior of $Al(NO_3)_3 \cdot 9H_2O$ and its Application in preparing Al_2O_3 and Regenerating HNO_3. *Process Saf. Environ. Prot.* **2023**, *178*, 728–738. [CrossRef]
11. Chen, Y.; Zhou, X.; Wan, S.; Zheng, R.; Tong, J.; Hou, H.; Wang, T. Synthesis and characterization of geopolymer composites based on gasification coal fly ash and steel slag. *Constr. Build. Mater.* **2019**, *211*, 646–658. [CrossRef]
12. Li, Z.; Zhang, Y.; Zhao, H.; Chen, H.; He, R. Structure characteristics and composition of hydration products of coal gasification slag mixed cement and lime. *Constr. Build. Mater.* **2019**, *213*, 265–274. [CrossRef]
13. Liu, T.; Awasthi, M.K.; Awasthi, S.K.; Ren, X.; Liu, X.; Zhang, Z. Influence of fine coal gasification slag on greenhouse gases emission and volatile fatty acids during pig manure composting. *Bioresour. Technol.* **2020**, *316*, 123915. [CrossRef] [PubMed]
14. Yuan, N.; Zhao, A.; Hu, Z.; Tan, K.; Zhang, J. Preparation and application of porous materials from coal gasification slag for wastewater treatment: A review. *Chemosphere* **2021**, *287*, 132227. [CrossRef] [PubMed]
15. Xiao, J.; Li, F.; Zhong, Q.; Bao, H.; Wang, B.; Huang, J.; Zhang, Y. Separation of aluminum and silica from coal gangue by elevated temperature acid leaching for the preparation of alumina and SiC. *Hydrometallurgy* **2015**, *155*, 118–124. [CrossRef]
16. Yang, Q.; Zhang, F.; Deng, X.; Guo, H.; Zhang, C.; Shi, C.; Zeng, M. Extraction of alumina from alumina rich coal gangue by a hydro-chemical process. *R. Soc. Open Sci.* **2020**, *7*, 192132. [CrossRef] [PubMed]
17. Dong, L.; Li, Y.; Yan, J.; Shu, X.Q. Efficient Extraction of SiO_2 and Al_2O_3 from Coal Gangue by Means of Acidic Leaching. *Adv. Mater. Res.* **2014**, *878*, 149–156. [CrossRef]
18. Cheng, F.; Cui, L.; Miller, J.D.; Wang, X. Aluminum Leaching from Calcined Coal Waste Using Hydrochloric Acid Solution. *Miner. Process. Extr. Metall. Rev.* **2012**, *33*, 391–403. [CrossRef]
19. Gaviría, J.; Bohé, A.; Pasquevich, A.; Pasquevich, D. Hematite to magnetite reduction monitored by Mössbauer spectroscopy and X-ray diffraction. *Phys. B Condens. Matter* **2007**, *389*, 198–201. [CrossRef]
20. Pineau, A.; Kanari, N.; Gaballah, I. Kinetics of reduction of iron oxides by H_2: Part I: Low temperature reduction of hematite. *Thermochim. Acta* **2006**, *447*, 89–100. [CrossRef]
21. Strangway, P.; Ross, H. The Kinetics of Hematite Reduction by Partially Reformed Natural Gas. *Can. Metall. Q.* **1966**, *5*, 221–235. [CrossRef]
22. Han, R.; Guo, X.; Guan, J.; Yao, X.; Hao, Y. Activation Mechanism of Coal Gangue and Its Impact on the Properties of Geopolymers: A Review. *Polymers* **2022**, *14*, 3861. [CrossRef] [PubMed]
23. Qin, Q.; Deng, J.; Geng, H.; Bai, Z.; Gui, X.; Ma, Z.; Miao, Z. An exploratory study on strategic metal recovery of coal gangue and sustainable utilization potential of recovery residue. *J. Clean. Prod.* **2022**, *340*, 130765. [CrossRef]
24. Guan, X.; Chen, J.; Zhu, M.; Gao, J. Performance of microwave-activated coal gangue powder as auxiliary cementitious material. *J. Mater. Res. Technol.* **2021**, *14*, 2799–2811. [CrossRef]
25. Guo, Y.; Yan, K.; Cui, L.; Cheng, F. Improved extraction of alumina from coal gangue by surface mechanically grinding modification. *Powder Technol.* **2016**, *302*, 33–41. [CrossRef]
26. Li, C.; Wan, J.; Sun, H.; Li, L. Investigation on the activation of coal gangue by a new compound method. *J. Hazard. Mater.* **2010**, *179*, 515–520. [CrossRef]
27. Han, L.; Ren, W.; Wang, B.; He, X.; Ma, L.; Huo, Q.; Wang, J.; Bao, W.; Chang, L. Extraction of SiO_2 and Al_2O_3 from coal gangue activated by supercritical water. *Fuel* **2019**, *253*, 1184–1192. [CrossRef]
28. Zhao, W.; Yang, B.; Yi, Y.; Feng, Q.; Liu, D. Synergistic activation of smithsonite with copper-ammonium species for enhancing surface reactivity and xanthate adsorption. *Int. J. Min. Sci. Technol.* **2023**, *33*, 519–527. [CrossRef]
29. Shen, Z.; Wen, S.; Wang, H.; Miao, Y.; Wang, X.; Meng, S.; Feng, Q. Effect of dissolved components of malachite and calcite on surface properties and flotation behavior. *Int. J. Miner. Metall. Mater.* **2023**, *30*, 1297–1309. [CrossRef]
30. Wang, Y.; Zhang, Y.; Zhou, Q.; Zhang, Y.; Sun, J. Thermal kinetics analysis of coal-gangue selected from Inner Mongolia in China. *J. Therm. Anal. Calorim.* **2018**, *131*, 1835–1843. [CrossRef]
31. Xu, B.; Liu, Q.; Ai, B.; Ding, S.; Frost, R.L. Thermal decomposition of selected coal gangue. *J. Therm. Anal. Calorim.* **2018**, *131*, 1413–1422. [CrossRef]
32. Madejová, J. FTIR techniques in clay mineral studies. *Vib. Spectrosc.* **2003**, *31*, 1–10. [CrossRef]
33. Hu, H.Y.P. Controlled coating of antimony-doped tin oxide nanoparticles on kaolinite particles. *Appl. Clay Sci.* **2010**, *48*, 368–374. [CrossRef]
34. Ion, R.M.; Radovici, C.; Fierascu, R.C.; Fierascu, I. Thermal and mineralogical investigations of iron archaeological materials. *J. Therm. Anal. Calorim.* **2015**, *121*, 1247–1253. [CrossRef]
35. Cheng, H.; Li, K.; Liu, Q.; Zhang, S.; Li, X.; Frost, R.L. Insight into the thermal decomposition of kaolinite intercalated with potassium acetate: An evolved gas analysis. *J. Therm. Anal. Calorim.* **2014**, *117*, 1231–1239. [CrossRef]
36. Shao, S.; Ma, B.; Wang, C.; Chen, Y. Thermal behavior and chemical reactivity of coal gangue during pyrolysis and combustion. *Fuel* **2023**, 331. [CrossRef]
37. Bi, H.; Wang, C.; Lin, Q.; Jiang, X.; Jiang, C.; Bao, L. Pyrolysis characteristics, artificial neural network modeling and environmental impact of coal gangue and biomass by TG-FTIR. *Sci. Total Environ.* **2021**, *751*, 142293. [CrossRef] [PubMed]
38. Guo, Y.; Zhao, Q.; Yan, K.; Cheng, F.; Lou, H.H. Novel Process for Alumina Extraction via the Coupling Treatment of Coal Gangue and Bauxite Red Mud. *Ind. Eng. Chem. Res.* **2014**, *53*, 4518–4521. [CrossRef]

39. Magdy, A.; Fouad, Y.; Abdel-Aziz, M.; Konsowa, A. Synthesis and characterization of Fe_3O_4/kaolin magnetic nanocomposite and its application in wastewater treatment. *J. Ind. Eng. Chem.* **2017**, *56*, 299–311. [CrossRef]
40. Yuan, S.; Zhou, W.; Han, Y.; Li, Y. Selective enrichment of iron particles from complex refractory hematite-goethite ore by coal-based reduction and magnetic separation. *Powder Technol.* **2020**, *367*, 305–316. [CrossRef]
41. Zhu, D.; Cui, Y.; Vining, K.; Hapugoda, S.; Douglas, J.; Pan, J.; Zheng, G. Upgrading low nickel content laterite ores using selective reduction followed by magnetic separation. *Int. J. Miner. Process.* **2012**, *106–109*, 1–7. [CrossRef]
42. Yuan, S.; Zhou, W.; Han, Y.; Li, Y. Efficient enrichment of low-grade refractory rhodochrosite by preconcentration-neutral suspension roasting-magnetic separation process. *Powder Technol.* **2020**, *361*, 529–539. [CrossRef]
43. Yuan, S.; Zhou, W.; Han, Y.; Li, Y. Selective enrichment of iron from fine-grained complex limonite using suspension magnetization roasting followed by magnetic separation. *Sep. Sci. Technol.* **2019**, *55*, 3427–3437. [CrossRef]
44. Li, X.-B.; Xiao, W.; Liu, W.; Liu, G.-H.; Peng, Z.-H.; Zhou, Q.-S.; Qi, T.-G. Recovery of alumina and ferric oxide from Bayer red mud rich in iron by reduction sintering. *Trans. Nonferrous Met. Soc. China* **2009**, *19*, 1342–1347. [CrossRef]
45. Qiao, X.C.; Si, P.; Yu, J.G. A Systematic Investigation into the Extraction of Aluminum from Coal Spoil through Kaolinite. *Environ. Sci. Technol.* **2008**, *42*, 8541–8546. [CrossRef] [PubMed]
46. Liu, X.; Liu, X.; Hu, Y. Investigation of the thermal behaviour and decomposition kinetics of kaolinite. *Clay Miner.* **2015**, *50*, 199–209. [CrossRef]
47. Omsinsombon, J.; Chaiyasat, A.; Busabok, C.; Chaiyasat, P. A novel iron aluminate composite polymer particle for high-efficiency self-coating solar heat reflection. *Sol. Energy Mater. Sol. Cells* **2021**, *230*, 111248. [CrossRef]
48. Jin, J.; Liu, X.; Yuan, S.; Gao, P.; Li, Y.; Zhang, H.; Meng, X. Innovative utilization of red mud through co-roasting with coal gangue for separation of iron and aluminum minerals. *J. Ind. Eng. Chem.* **2021**, *98*, 298–307. [CrossRef]
49. Yamashita, T.; Hayes, P. Analysis of XPS spectra of Fe^{2+} and Fe^{3+} ions in oxide materials. *Appl. Surf. Sci.* **2008**, *254*, 2441–2449. [CrossRef]
50. Fang, S.; Xu, L.; Wu, H.; Xu, Y.; Wang, Z.; Shu, K.; Hu, Y. Influence of surface dissolution on sodium oleate adsorption on ilmenite and its gangue minerals by ultrasonic treatment. *Appl. Surf. Sci.* **2020**, *500*, 144038. [CrossRef]
51. Omran, M.; Fabritius, T.; Elmahdy, A.M.; Abdel-Khalek, N.A.; El-Aref, M.; Elmanawi, A.E.-H. XPS and FTIR spectroscopic study on microwave treated high phosphorus iron ore. *Appl. Surf. Sci.* **2015**, *345*, 127–140. [CrossRef]
52. Salama, W.; El Aref, M.; Gaupp, R. Spectroscopic characterization of iron ores formed in different geological environments using FTIR, XPS, Mössbauer spectroscopy and thermoanalyses. *Spectrochim. Acta Part A Mol. Biomol. Spectrosc.* **2015**, *136*, 1816–1826. [CrossRef]
53. Dong, H.; Du, W.; Dong, J.; Che, R.; Kong, F.; Cheng, W.; Ma, M.; Gu, N.; Zhang, Y. Depletable peroxidase-like activity of Fe_3O_4 nanozymes accompanied with separate migration of electrons and iron ions. *Nat. Commun.* **2022**, *13*, 5365. [CrossRef] [PubMed]
54. Grosvenor, A.; Kobe, B.; McIntyre, N. Examination of the oxidation of iron by oxygen using X-ray photoelectron spectroscopy and QUASESTM. *Surf. Sci.* **2004**, *565*, 151–162. [CrossRef]
55. Liu, H.; Zhang, S.; Yang, W.; Yu, N.; Liu, C.; Chai, Y.; Dong, B. Directional Reconstruction of Iron Oxides to Active Sites for Superior Water Oxidation. *Adv. Funct. Mater.* **2023**, *33*, 2303776. [CrossRef]
56. Gu, A.; Chen, K.; Zhou, X.; Gong, C.; Wang, P.; Jiao, Y.; Mao, P.; Chen, K.; Lu, J.; Yang, Y. Trimetallic MOFs-derived Fe-Co-Cu oxycarbide toward peroxymonosulfate activation for efficient trichlorophenol degradation via high-valent metal-oxo species. *Chem. Eng. J.* **2023**, *468*, 143444. [CrossRef]
57. Li, X.; Wang, H.; Zhou, Q.; Qi, T.; Liu, G.; Peng, Z. Efficient separation of silica and alumina in simulated CFB slag by reduction roasting-alkaline leaching process. *Waste Manag.* **2019**, *87*, 798–804. [CrossRef]
58. Zhou, Q.-S.; Li, C.; Li, X.-B.; Peng, Z.-H.; Liu, G.-H.; Qi, T.-G. Reaction behavior of ferric oxide in system Fe_2O_3–SiO_2–Al_2O_3 during reductive sintering process. *Trans. Nonferrous Met. Soc. China* **2016**, *26*, 842–848. [CrossRef]
59. Zhang, Y.; Xu, L.; Seetharaman, S.; Liu, L.; Wang, X.; Zhang, Z. Effects of chemistry and mineral on structural evolution and chemical reactivity of coal gangue during calcination: Towards efficient utilization. *Mater. Struct.* **2014**, *48*, 2779–2793. [CrossRef]
60. Zhang, C.; Yang, X.Y.; Li, Y.F. Mechanism and Structural Analysis of the Thermal Activation of Coal-Gangue. *Adv. Mater. Res.* **2011**, *356–360*, 1807–1812. [CrossRef]
61. Kong, D.; Zhou, Z.; Song, S.; Feng, S.; Lian, M.; Jiang, R. Preparation of Poly Aluminum-Ferric Chloride (PAFC) Coagulant by Extracting Aluminum and Iron Ions from High Iron Content Coal Gangue. *Materials* **2022**, *15*, 2253. [CrossRef] [PubMed]
62. Zhang, T.A.; Han, X.; Lv, G.; Pan, X.; Agajan, S.; Fu, D.; Liu, J.; Zhang, J. Research on Alumina Preparation from Aluminium Chloride Solution by Electrolysis Process. In *Light Metals 2018, Proceedings of the TMS 2018, Phoenix, AZ, USA, 11–15 March 2018*; Martin, O., Ed.; Springer International Publishing: Cham, Switzerland, 2018; pp. 97–103. [CrossRef]
63. Asuha, S.; Talintuya, T.; Han, Y.; Zhao, S. Selective extraction of aluminum from coal-bearing kaolinite by room-temperature mechanochemical method for the preparation of γ-Al_2O_3 powder. *Powder Technol.* **2018**, *325*, 121–125. [CrossRef]
64. Kong, D.; Jiang, R. Preparation of NaA Zeolite from High Iron and Quartz Contents Coal Gangue by Acid Leaching—Alkali Melting Activation and Hydrothermal Synthesis. *Crystals* **2021**, *11*, 1198. [CrossRef]
65. Liu, S.; Chen, X.; Ai, W.; Wei, C. A new method to prepare mesoporous silica from coal gasification fine slag and its application in methylene blue adsorption. *J. Clean. Prod.* **2019**, *212*, 1062–1071. [CrossRef]

66. Li, C.-C.; Qiao, X.-C.; Yu, J.-G. Large surface area MCM-41 prepared from acid leaching residue of coal gasification slag. *Mater. Lett.* **2016**, *167*, 246–249. [CrossRef]
67. *GB/T 212-2008*; Proximate Analysis of Coal. China Coal Industry Association: Beijing, China, 2008.

Disclaimer/Publisher's Note: The statements, opinions and data contained in all publications are solely those of the individual author(s) and contributor(s) and not of MDPI and/or the editor(s). MDPI and/or the editor(s) disclaim responsibility for any injury to people or property resulting from any ideas, methods, instructions or products referred to in the content.